Journal of Statistical Mechanics:
Theory and Experiment

PAPER: CLASSICAL STATISTICAL MECHANICS, EQUILIBRIUM AND NON-EQUILIBRIUM

Clogging in two-dimensions: effect of particle shape

Journal of Statistical Mechanics: Theory and Experiment
An IOP and SISSA journal

PAPER: Classical statistical mechanics, equilibrium and non-equilibrium

Clogging in two-dimensions: effect of particle shape

Ezequiel Goldberg[1], **C Manuel Carlevaro**[1,2] **and Luis A Pugnaloni**[3]

[1] Universidad Tecnológica Nacional—FRBA, UDB Física, Mozart 2300, C1407IVT Buenos Aires, Argentina
[2] Instituto de Física de Líquidos y Sistemas Biológicos (CONICET La Plata, UNLP), Calle 59 Nro 789, 1900 La Plata, Argentina
[3] Dpto. Ingeniería Mecánica, Facultad Regional La Plata, Universidad Tecnológica Nacional, CONICET, Av. 60 Esq. 124, 1900 La Plata, Argentina
E-mail: luis.pugnaloni@frlp.utn.edu.ar

Received 31 July 2018
Accepted for publication 3 October 2018
Published 9 November 2018

Online at stacks.iop.org/JSTAT/2018/113201
https://doi.org/10.1088/1742-5468/aae84b

Abstract. We study the discharge of a two-dimensional silo through small openings via discrete element simulations. We consider the effect of the shape of the grains on the clogging of the flow, focusing on regular polygons and disks. We show that the clogging probability presents a non-linear response as a function of the number of vertexes of the polygons. Also, the clogging probability is strongly dependent on the protocol used to trigger the flow after each clog. We found that the size and shape of the blocking arches display a much larger variability for some polygons, particularly for squares, than for disks.

Keywords: avalanches, granular matter, clogging

1742-5468/18/113201+18$33.00

Contents

1. Introduction

In a number of industrial applications, granular materials are made to flow through a constriction to feed the next stage of a process. If the aperture is small, clogging is likely. This phenomenon produces undesirable interruption, for example in production lines. One may avoid clogging by using larger apertures, but this increases the flow rate, which may be a drawback for some equipment. For spherical grains, a circular opening larger than five particle diameters will rarely clog [1]. Whether this is a sharp transition between clogging and continuous flow regimes is still under debate [2–4]. For a review on clogging through bottlenecks see [5].

Vibration of the equipment prone to clogging is a suitable mean to reduce the impact of jams. It has been observed that vibration does not prevent clogging to happen, but clogging arches do get destabilized and the flow is soon resumed [6]. A number of recent studies focus on the duration of clogs during vibration, either externally induced [6–8] or by intrinsic vibration in self-propelled particles [8–10].

The shape that clogging arches display for circular grains in two-dimensional (2D) hoppers was originally modeled by To *et al* [11]. Later on, Garcimartín *et al* compared the geometrical characteristics of clogging arches in a quasi-two-dimensional experiment with those of arches found in the interior of a granular pack and with To's predictions [12]. The overall findings were that the constrained random walk model from To *et al* overestimated the spread of possible arch spans. The shape of the experimental arches of disks approached a circle when the number of particles was large (typically three or more particles in excess of the minimum necessary to clog) compared with the size of the aperture that they clogged.

J. Stat. Mech. (2018) 113201

One interesting feature of clogging is that friction seems to play little part in its likelihood [1]. However, the total lack of friction does reduce the clogging probability drastically [13, 14] and the influence of the column height becomes relevant [15]. Moreover, frictionless soft particles present a wide range of clogging probabilities. One should also expect that the shape of the grains is a key factor for the ability of grains to clog. Indeed, Zuriguel *et al* [1] and more recently Ashour *et al* [16] have shown that anisotropic grains present a larger tendency to clogging in comparison with spheres. One important factor in these grains is the fact that they align their long axis in the radial direction with the center of the aperture while they flow.

In this work, we present results of 2D simulations of grains with shape of regular polygons (triangles, squares, pentagons, hexagons and heptagons) in addition to circular grains. These particles are not different to each other because of their anisotropy but due to the number of edges they present for interaction and the rotational constraints that this may impose. We focus on the clogging events during the discharge of the grains through small openings in the base of a static (not vibrated) flat bottom silo. To compare results from different shapes, we use as a criterion that the grains must have the same mass. We will show that the intuitive prediction that polygonal grains are more prone to clogging than disks is indeed confirmed. However, there are some exceptions to this rule. Moreover, there is not a monotonic relation between the number of vertexes of a polygon and its tendency to clogging. We have also considered the effect of triggering the flow after each clog using different protocols. The results show that the protocol is very important in the results and should be carefully chosen when comparing results from different laboratories.

2. Simulation

We simulate a 2D silo by means of a discrete element method (DEM) using the Box2D library [17]. This package uses a constraint solver. At each time step of the dynamics, a series of iterations (typically 20) are used to resolve penetrations between bodies through a Lagrange multiplier scheme [18]. After detecting overlaps, the inelastic collision at each contact is solved and new linear and angular velocities are assigned. The equations of motion are integrated through a symplectic Euler algorithm. The time step δt used to integrate the equations of motion is $0.025\sqrt{d/g}$; with $d = 1\,\mathrm{cm}$ the diameter of our circular grains and $g = 9.8\ \mathrm{m\ s^{-2}}$ the acceleration of gravity. Solid friction is also handled by means of a Lagrange multiplier scheme that implements the Coulomb criterion. Box2D has been previously used to simulate continuous silo discharges [19], and tapping of granular systems [20].

Grains of different shapes corresponding to regular polygons (triangles, squares, pentagons, hexagons and heptagons) are used in the simulations apart from the circular grains. All grains have the same material density ($0.01\,\mathrm{kg\ m^{-2}}$) and the same area, hence the same weight. Each simulation contains only one type of grain and these are monosized. The restitution coefficient is set in all cases to $\epsilon = 0.05$ and the friction coefficient μ is set to 0.5. The interaction parameters between the grains and the silo

J. Stat. Mech. (2018) 113201

are the same as the grain–grain interaction. The significantly low restitution coefficient allows for a rapid dissipation of the kinetic energy during the initial filling of the silo.

The silo consists of a rectangular box $20d$ wide and $180d$ high, with its base positioned at $y = 0$ (the vertical direction) and centered at $x = 0$ (the horizontal direction). Gravity acts in the negative vertical direction. 2000 grains are used in each discharge. After grains initially placed at random without overlaps settle, an aperture of width σ (we define $D = \sigma/d$ as the ratio between the aperture width and diameter of the circular grains) opened at the center of the flat base of the silo allows the grains to discharge. For small apertures, clogging is observed. We consider a clog is permanent if more than 5 s have passed without any grain falling through the aperture. For each clog, we record the number of particles that passed through the aperture. We call this an avalanche. We record, for each aperture size and for each grain shape, 3000 clogs. After clogging, a snapshot of the static configuration is saved (including the information of the pairs of particles in contact) for the analysis of the blocking arch. This is done only for 150 clogs for each orifice and particle shape.

We use two alternative methods to resume the flow after a clogging event. In the method that we call *global* perturbation, we carry out a new simulation by filling a new silo using different random initial positions for the grains after each clog [21]. For the method that we call *local* perturbation, we unclog the system by removing some particles from the blocking arch and reinjecting them on top of the silo. The particles to remove are selected by finding all grains for which the segment that joins the center of the grain with the center of the orifice does not intersect any other grain. Moreover, during the flow of an avalanche, particles in the local perturbation method are also reinjected at the top of the silo as soon as they leave through the bottom opening. This allows the recording of extremely large avalanches observed for large orifices. For the global perturbation we did not reinject the particles; therefore, the silo can fully empty without clogging for large openings. These events where registered and duly accounted for in the statistics.

The local perturbation approach is similar to the one used in most experimental studies. After each clog, the flow is usually resumed by disturbing the arch blocking the aperture (for example using an air jet [22]). However, some other studies simply empty the container and carry out a new fill-flow-clog sequence [11], similar to our global perturbation approach. In some simulation studies, where the effect of the initial packing fraction was of particular interest, the system had to be filled and prepared in the container from scratch before triggering each avalanche to warrant that the proper packing fraction was set [23]. Here, we will assess the impact of the results due to the perturbation method used.

3. Arch detection

The concept of arch in granular systems seems, at first glance, rather intuitive. However, a rigorous definition is still lacking. The most accepted definition is that an arch (not to be confused with force chain) is a set of grains that support each other. This leads to a natural definition in terms of pair-wise stability: two grains A and B are mutually

J. Stat. Mech. (2018) 113201

stable if A supports B and B supports A. Then, two grains in any packing are part of the same arch if there is a chain of mutually stable particles that connects them [24, 25]. However, defining if a particle A is or not supported by a particle B is not trivial. An algorithm has be developed for DEM simulations that shows that a simple snapshot is not sufficient and the full history of each contact must be known [26].

For the particular case of an arch that blocks an orifice, the definition is expected to be much simpler since this arch usually lacks grains underneath that complicate the analysis of many contacts. A reasonable definition can be achieved even without resorting to a history dependent algorithm. In particular, Garcimartín *et al* have developed an algorithm to detect a blocking arch in a simple image of the clogged system [12]. We have attempted to use this algorithm, however, the non-circular shapes of our grains introduced additional complexity to the problem and we had to develop a more sophisticated analysis. In particular, polygonal grains tend to show very complex shapes with concave and convex sections, plus the ability to interlock in very large structures below which small groups of grains can still remain on the base, next to the orifice.

After trying different algorithms, we selected the one that seemed to detect as the blocking arch the most sensible group of grains by visual inspection. The algorithm takes the network defined by the particle centers as the nodes, with the bonds between the nodes drawn for each pair of grains in contact. Then, all grains touching the base (at the left and right side of the orifice) are detected. Then, all paths through the network between the left grains and right grains are identified. From these paths, the one with fewest nodes is selected. In some cases, this selection is not unique. When this happens, we chose among the shortest paths the one that has the grains with lowest vertical coordinate. Finally, we consider that only a portion of the particles in the selected path are part of the blocking arch. Some of these particles may be simply supported by the base at each side of the orifice and do not really constitute part of the arch. To select the particles that form the arch itself we follow the path starting at the 'central' grain whose x coordinate is closer the the center of the orifice. Then, following the path to the right, we add grains to the arch until one grain has its x coordinate to the left of the previous in the list. Finally, we follow the path to the left of the 'central' grain and add grains until one particle has its x coordinate to the right of the previous in the list. Examples of detected arches in a variety of conditions are shown in figure 1. As we can see, the algorithm can detect arches in rather complex configurations.

4. Results

4.1. Avalanche size distribution

The distribution of avalanche sizes $n_s(D)$ is defined as the fraction of avalanches of s grains [11]. As we mentioned, one avalanche is the flow of grains from the triggering of the flow until the next clogging event. This distribution depends on the size of the aperture since a larger D leads to larger avalanches in average. In general, for rounded particles, $n_s(D)$ shows an exponential tail as a function of s [11, 22, 27]. Elongated and prolate grains in 3D have shown power-law tails [1].

J. Stat. Mech. (2018) 113201

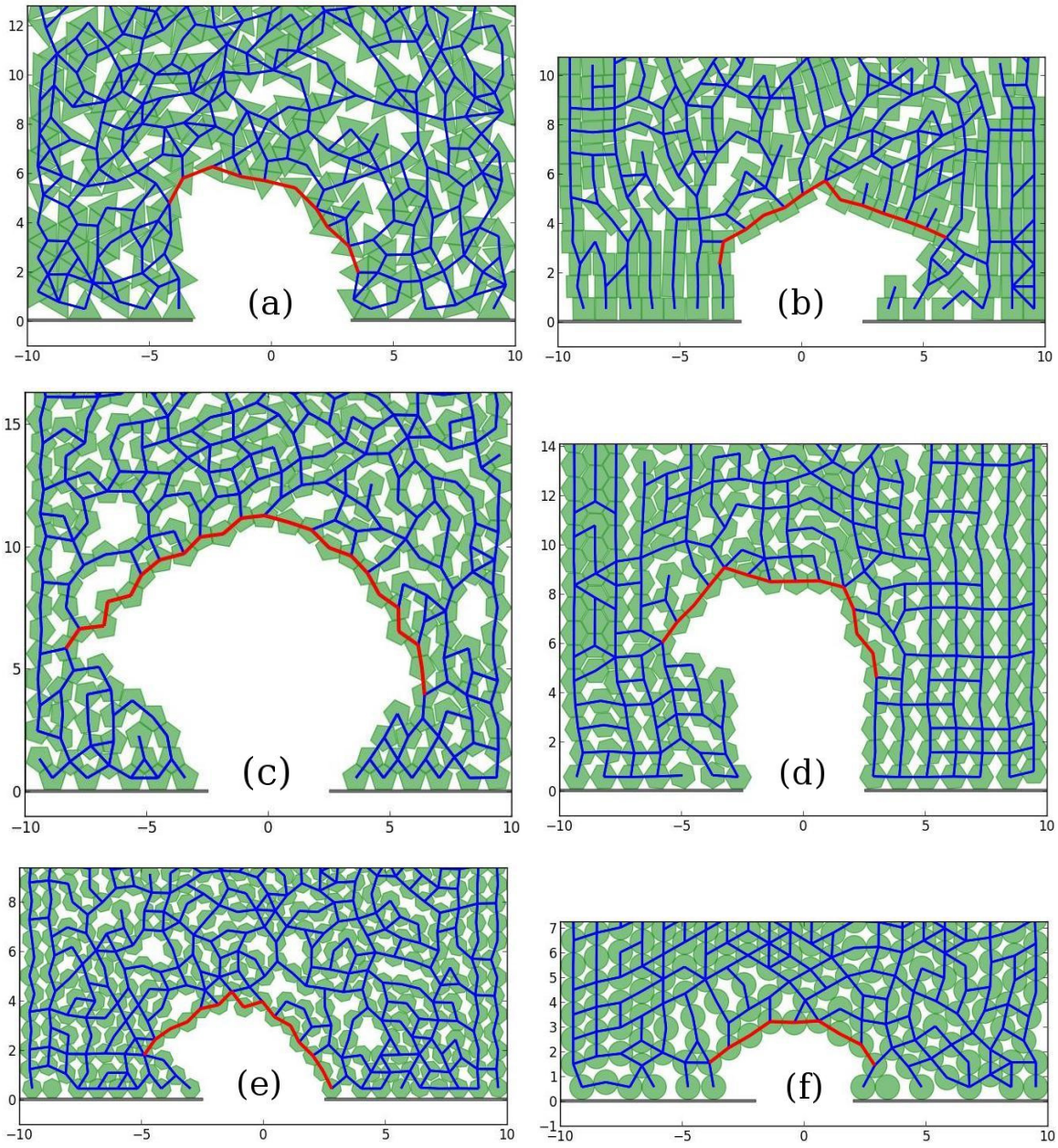

Figure 1. Snapshots of clogged configurations with clogging arch detected for different grain shapes: (a) triangles, (b) squares, (c) pentagons, (d) hexagons, (e) heptagons, and (f) disks. The blue segments correspond to the network of contacts saved during the simulations. The red segments correspond to the blocking arch detected by the algorithm described in the text. The length scales are in units of d.

Our polygonal grains display exponential tails for $n_s(D)$. Figure 2 presents n_s for an aperture $D = 4.0d$, for each grain shape for both perturbation protocols. For the local perturbation, figure 2(a) shows that the avalanches are typically smaller for triangles (more prone to clogging) and larger for heptagons and disks. Squares, pentagons and hexagons have similar avalanche distributions, with sizes in between triangles and disks. Heptagons present a distribution very close to the one for disks. This may suggest that heptagons are 'round enough' to mimic the behavior of disks, however this

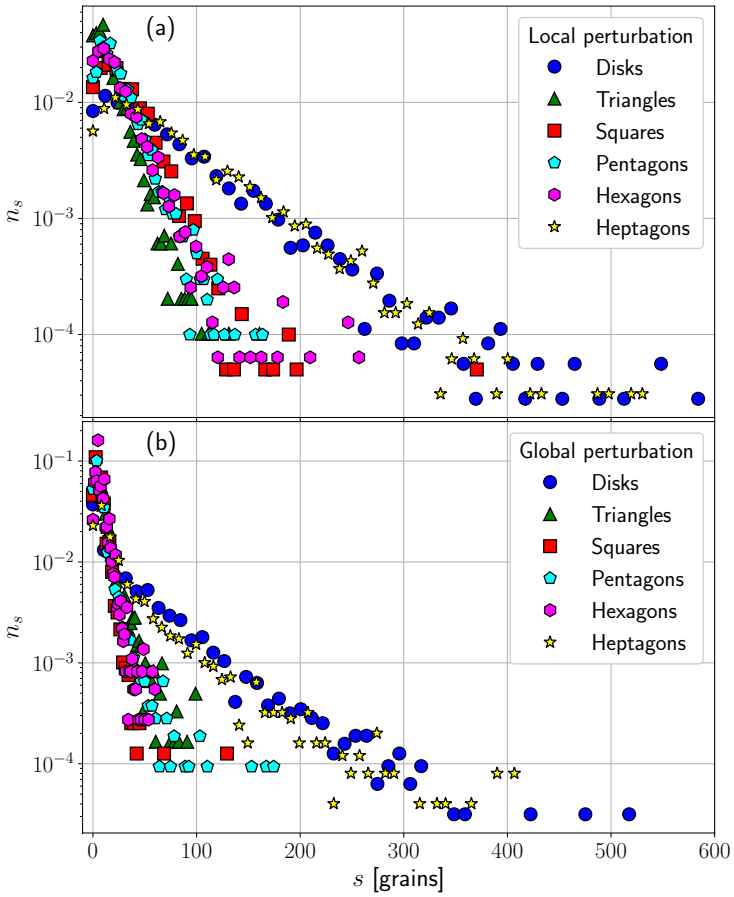

Figure 2. Distribution of avalanche sizes $n_s(D)$ for an aperture of width $D = 4.0$ for different grain shapes (see legend). (a) Local perturbation protocol. (b) Global perturbation protocol.

agreement is less perfect for other orifices diameters (for a detailed discussion on the clogging probability as a function of D see next section).

The use of a global rearrangement to generate a new avalanche leads to smaller avalanches. In figure 2(b), we see that the exponential tail is conserved for the global perturbation. However, for disks and heptagons, for example, avalanches larger than 50 grains are systematically more probable in the local perturbation (figure 2(a)) than in the global perturbation protocol. Moreover, for global perturbations, the squares yield the smaller avalanches in average instead of the triangular grains. We will come back to explain this peculiar swap between triangles and squares after we consider the shape of arches in section 4.3.

The mean avalanche size as a function of D^2 is shown in figure 3 for both perturbation protocols. Since in the global perturbation we have not reinjected grains during the avalanches, the silo often empties before clogging at large aperture sizes. We have therefore considered only small apertures for this case, for which this penomenon is not observed. The mean avalanche size for the global perturbation is significantly smaller than for the local perturbation, regardless of the grain shape. See section 4.3 for an explanation of this effect.

J. Stat. Mech. (2018) 113201

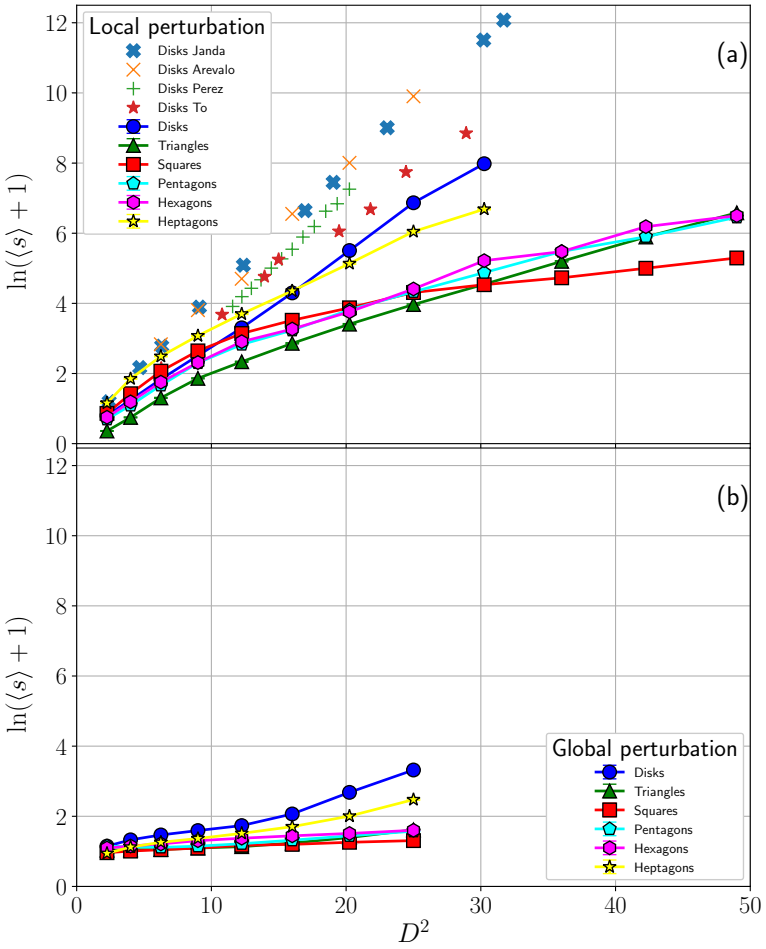

Figure 3. Mean avalanche size S as a function of D^2 for the different particle shapes and for the global (a) and local (b) perturbation protocols. We compare with the experimental results by Janda *et al* [7] and To [27] and the simulations by Arévalo *et al* [30] and Perez [29] carried out in 2D. Error bars are smaller than the size of the symbols and indicate the standard error of the mean.

For disks, there have been a number of studies (both experimental [2, 27] and numerical [29, 30]) where the mean avalanche size has been reported. Most studies use protocols to trigger avalanches similar to the the local perturbation we use here. In figure 3(a) we include the results by these authors. As we can see, our mean avalanche sizes are smaller than in all previous studies, although within the confidence interval if compared with the experiments of [27]. It is unclear to us what is the origin of the discrepancies in the literature; however, we can mention a few possible sources. First, the protocol used to trigger the avalanches may vary from one study to the other and this should be an important factor. Second, Gella *et al* [28] have shown that there is a small influence of the 2D silo width on the avalanches. In fact, our silo is 20 particles across, which seems to yield the minimum mean avalanche size [28]. It is worth mentioning, however, that Arévalo *et al* [30] used a silo similar to ours, but our results do not agree with theirs. Third, Uñac *et al* [23] have shown that the mean avalanche size depends on the initial packing fraction before starting the avalanche. High packing

J. Stat. Mech. (2018) 113201

fractions tend to deliver smaller avalanches. There is little information of the packing fraction for the clogging studies in the literature to asses to what degree this effect can explain the discrepancies.

In figure 3(a) we can see that the effect of the grain shape on the mean avalanche size is dramatic in most cases. Although heptagons display avalanches similar to disks, all other particle shapes induce smaller avalanches. Moreover, disks show a linear growth in the logarithmic plot as a function of D^2, as discussed in previous studies [2, 27], whereas triangles, squares, pentagons and hexagons present a sub-linear growth. To appreciate the strong differences, notice that to obtain similar avalanches to the ones observed for disks at $D = 5.0$ it requires that triangles, pentagons and hexagons be discharged though an aperture with $D = 7.0$ (i.e. 40% larger). Interestingly, in a previous study on the continuous flow regime of polygonal grains, for larger apertures, we showed that to achieve a flow rate similar to disks, polygonal grains only need to flow through orifices 20%–25% larger [19].

4.2. Clogging probability

The clogging probability $J_N(D)$ is defined as [22]

$$J_N(D) = \sum_{s=0}^{N-1} n_s(D). \tag{1}$$

$J_N(D)$ corresponds to the probability that an avalanche smaller than N grains discharges through an aperture of size D before the system clogs. Figure 4 shows $J_{50}(D)$ for different grain shapes and the two perturbation protocols. As observed in previous studies, $J_N(D)$ is one for small D and falls to zero when D increases. We also observed, in agreement with previous works, that an increase in N leads to a shift of the curves to the right, indicating a larger probability of jamming before N grains flow freely (data not shown). When comparing the two different protocols, we observe that the local perturbation yields, systematically for any given polygon, a lower clogging probability than the global perturbation. The reason for this is that, for the local perturbation, flow is triggered from a configuration that has an arch at the aperture. This leads to a rapid initial flow of a low density region just above the outlet that has low chances to clog. In contrast, the global perturbation starts each avalanche with the container filled anew and the aperture closed. Hence, the opening of the orifice finds the nearby region with a high packing fraction and the likelihood of clogging is larger.

Figure 4(a) shows that, for the local perturbation, heptagons are about as likely to clog as disks for all aperture sizes. Squares are significantly more likely to clog than disks. Then, pentagons and hexagons are similar in clogging probability and above squares. Finally, triangles are the most likely to clog as we suggested in the previous section. $J_N(D)$ allow us to see that for some apertures the order of clogging likelihood amongst polygons may change slightly. For example, there is a swap between disks and heptagons at about $D/d = 4.25$, and also a swap between squares and pentagons/hexagons at $D/d \approx 5.25$. This changes are small, but they indicate that the order of clogging likelihood heptagons—disks—squares—pentagons—hexagons—triangles should be considered as a rule of thumb and not a precise order. One may be tempted to find plausible arguments for triangles to be so prone to clogging in comparison with other

J. Stat. Mech. (2018) 113201

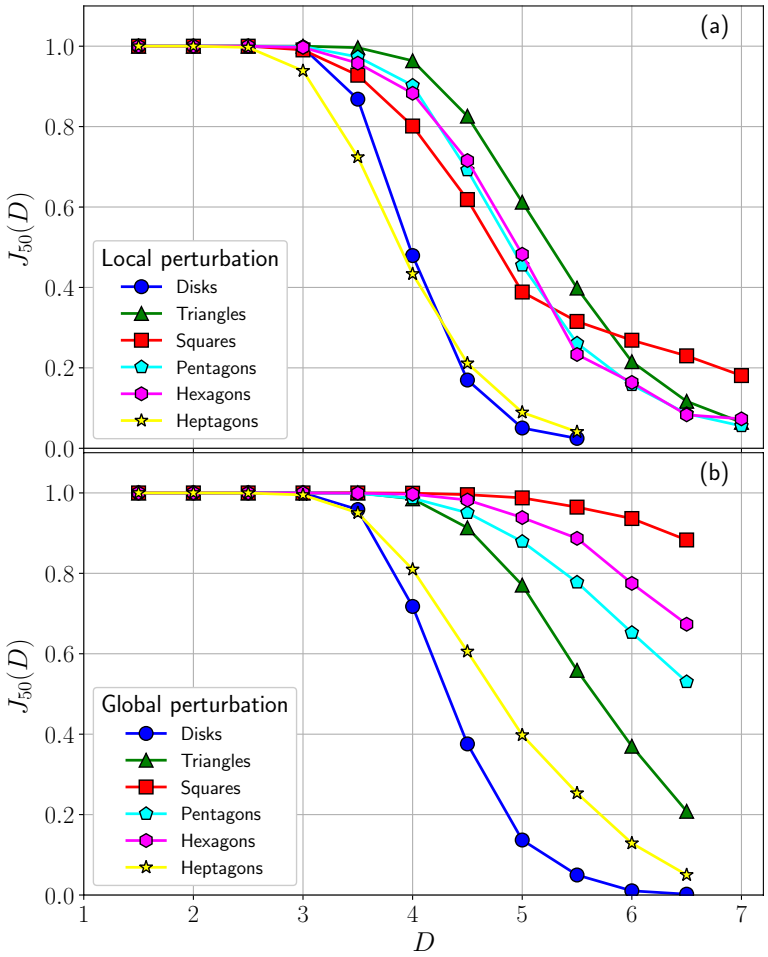

Figure 4. Clogging probability as a function of D for the different grain shapes for $N = 50$. (a) Local perturbation, and (b) global perturbation protocol.

shapes. However, this may become a pointless exercise in view of the results obtained with a different protocol for unclogging that yields dramatic changes in the relative response of different polygons as we discuss below.

Figure 4(b) shows $J_{50}(d)$ for the global perturbation protocol. Here, squares (and not triangles) have the largest tendency to clogging. In fact, triangles are fourth in the list of decreasing clogging probability after squares, hexagons and pentagons. In contrast to the local perturbation results, the global perturbation shows that disks are the less likely to clog. Then, the order in clogging likelihood is disks—heptagons—triangles—pentagons—hexagons—squares. This is dramatically different to the results obtained with the local perturbation protocol. Hence, any interpretation on the underlying mechanisms for the enhancement of clogging when disks are replaced by different regular polygons would require considerations on the protocol used to trigger avalanches. After discussing the shape of the arches that block the aperture in the next section, we will provide some clues for the peculiar swap in the order of clogging probability observed between triangles and squares when we change the perturbation mechanism.

As we can see from figure 4, the clogging probability is non-monotonic with the number of vertexes. A non-linear behavior on the number of vertexes of the grains has

J. Stat. Mech. (2018) 113201

also been found in the packing fraction of tapped columns of regular polygons [20] and tapped packings of aggregates [31]. However, the packing fraction is significantly determined by the ability of a polygonal shape to tessellate the space, and one can naturally expect that tessellating shapes will yield higher packing fractions. In the case of clogging, the ability of interlocking thanks to the vertexes seems to be more important than the ability of tessellating the space.

4.3. Side-to-side contacts

One may speculate that clogging can be connected with the ability of polygonal particles to form side-to-side contacts in contrast to vertex-to-side or vertex-to-vertex contacts. To asses this in a first order approximation, we have calculated the fraction of side-to-side contacts in the pack of particles inside the silo after each clog for the local perturbation protocol (see figure 5). As we can see, the fraction of side-to-side contacts increases with D. This is most probably due to the fact that large apertures induce longer periods of flow which in turn favors the rearrangement of particles and the formation of side-to-side contacts.

When comparing results for different particle shapes, one immediately sees that the tendency to form side-to-side contacts is not directly correlated with the clogging probability. For example, triangles and pentagons present a similar fraction of side-to-side contacts but their clogging probabilities are clearly different (see figure 4(a)). Likewise, pentagons and hexagons show very similar clogging probabilities, yet they have remarkably different fractions of side-to-side contacts.

We cannot conclude that there is a simple connection between clogging probability and the ability of the grains to form flat contacts. However, it may be the case that the clogs formed are more stable if side-to-side contacts are present. Although there is a number of studies on the stability of arches (e.g. disturbed by vibrations [32, 33]), none has considered the effect of particle shape on their stability. However, such study is beyond the goals of this paper.

4.4. Shape of arches

For the simulations with the local perturbation protocol, we have detected each particle that forms part of a blocking arch by using the procedure described in section 3. For these arches, a number of structural descriptors can be extracted. The average number of grains in an arch, as a function of the aperture size, is plotted in figure 6. In general, triangles form arches with fewer particles than any other shape, including disks. This is due to the ability of triangles to fit their acute vertexes in the aperture and lock with neighboring vertexes and the orifice edges. The other polygons tend to form arches with more particles than the disks. This is expected since interlocking should be enhanced by the presence of vertexes. Moreover, the spread in the distribution of number of particles is much wider than for disks or triangles. This is particularly evident in the case of squares (see error bars in figure 6). We can see that the clogging arches reported by Garcimartín *et al* [12] for experiments carried out with spherical particles confined in a quasi-two-dimensional geometry seem to be smaller than the ones detected here. However, in [12] the definition of the arch excluded the two grains

J. Stat. Mech. (2018) 113201

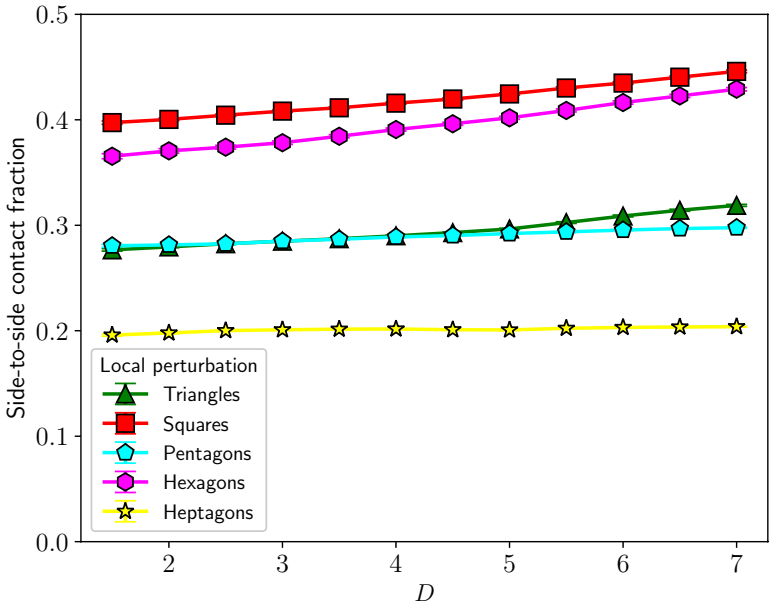

Figure 5. Fraction of side-to-side contacts in the silo after each clog for the various particle shapes as a function of the aperture width.

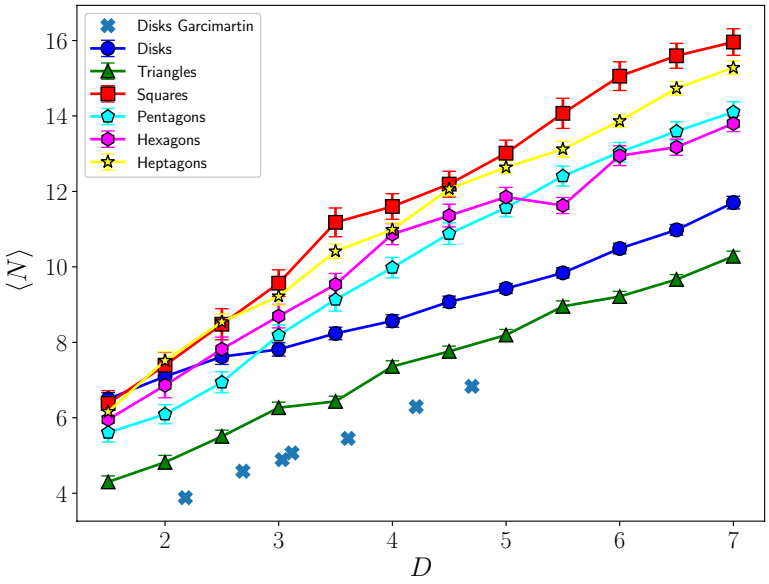

Figure 6. Average number of particles in the arch that blocks an orifice of size D. Error bars correspond to error of the mean (estimated as $std/\sqrt{N_{\text{arch}}}$, being std the standard deviation and N_{arch} the number of arches averaged). The light blue crosses correspond to the results of [12] for spherical grains in a quasi-two-dimensional geometry.

that touched the base in all cases. In our definition these two particles can be part of the arch. As a consequence, our mean number of grains for disks is about two grains in excess of that reported by Garcimartín *et al*. This difference is less marked for large orifices since in such cases arches tend to rest on top of stable particles at each side of the aperture and less frequently extend down to the base (see for example figure 1(f)).

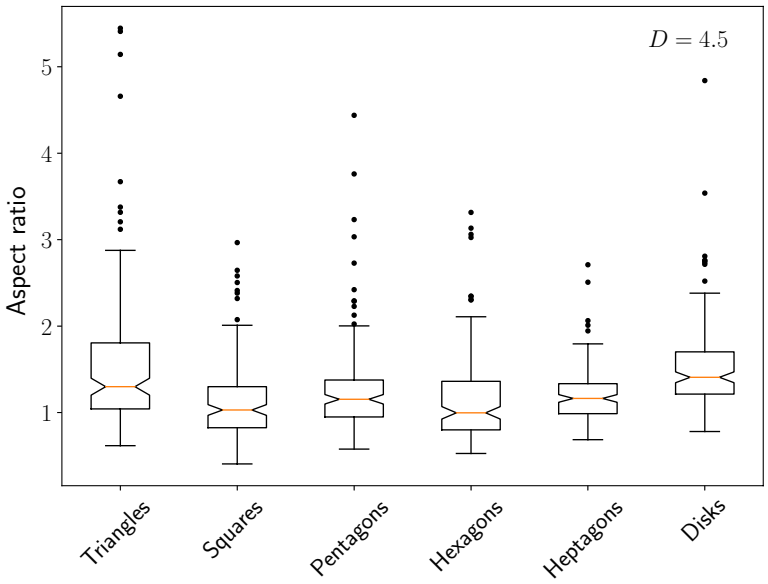

Figure 7. Notched box plot of the distribution of the aspect ratios of the arches for the various particle shapes using an aperture $D = 4.5$.

In figure 7 we show the distribution of the aspect ratios of the arches using notched box diagrams. The aspect ratio is defined, following Garcimartín *et al* [12], as half the horizontal distance between the centers of the leftmost and rightmost particles divided by the vertical distance between the centers of the lower and upper particles of the arch. As we can see, for disks, the median aspect ratio is about 1.5, which is consistent with the results in [12]. With the exception of triangles, which present a distribution of aspect ratios similar to disks, all other shapes display a lower aspect ratio. This means that arches are typically taller (for a given width) for all polygons in comparison with disks and triangles. In particular, squares and hexagons show a considerable number of arches with aspect ratios below one, which indicates that these particle shapes have a larger tendency to form tall arches.

We have considered a number of additional geometrical characteristics of the arches, such as tortuousness and span. However, we focus here on a measure of the vertical placement of the arch since this property seems to be rather sensitive to particle shape and helps to understand the dramatic differences in clogging probability for the two perturbation protocols. Figure 8 shows the vertical position y_{cm} of the center of mass of the arches (averaged over all arches). Notice that many arches may be formed by few particles but be located at a high position spanning the space between the two stable piles of particles resting on each side of the aperture. A good example of these types of arrangements can be seen in figure 1(d). As we can see, squares form arches at very high placements. This is due to the fact that squares can pile up with a rather high internal angle in comparison with other polygons. This can build a very narrow vertical channel that can be clogged with high probability at many different heights, as it has been shown in vertical pipe experiments [34]. This effect leads to a very spread distribution in the arch vertical position for squares as it can be observed in the notched box plot of figure 8(b). Disks, heptagons and triangles tend to form arches close to the opening;

J. Stat. Mech. (2018) 113201

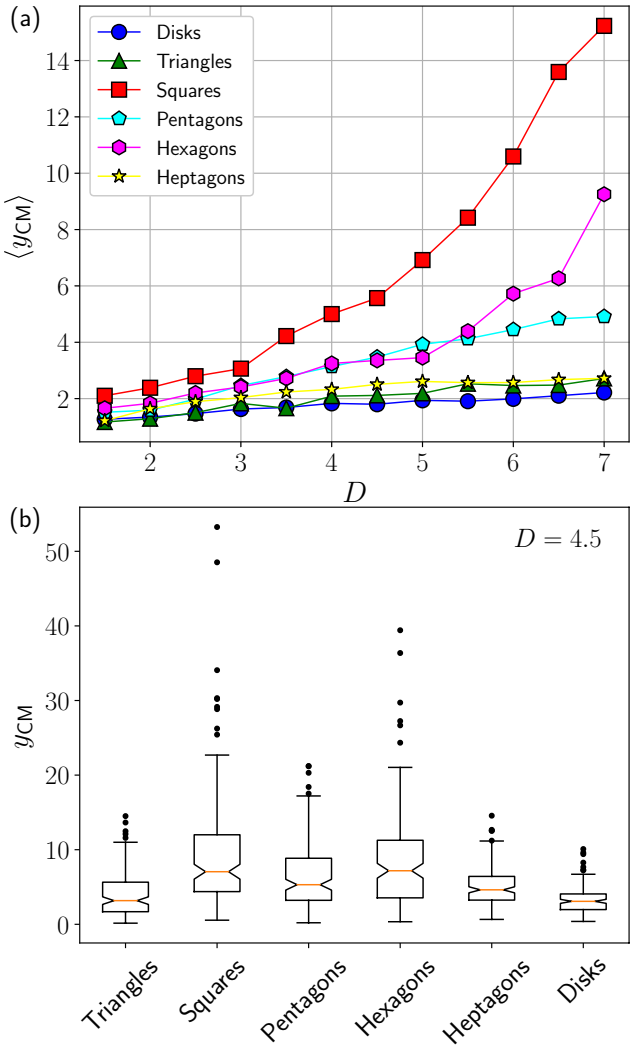

Figure 8. (a) Vertical position y_{cm} of the center of mass of the arches as a function of D for different particle shapes. (b) Notched box plot of the distribution of y_{cm} for each particle shape using $D = 4.5$.

while hexagons, pentagons, and especially squares tend to form blocking arches further up in the granular column.

The observations on the vertical placement of arches allow us to understand the major differences between figures 4(a) and (b). Apart from the overall increase in clogging probability observed for the global perturbation, we see that squares and triangles swap their relative position in clogging likelihood when the perturbation protocol is changed. As we mentioned, squares tend to form blocking arches at very high placements. If an avalanche is triggered from a previous arch (local perturbation), squares will fall from a high position through an empty channel and a fair number of grains will exit before a new arch arrests the flow; resulting in a lower $J_N(D)$ than that expected from the global perturbation where the system is packed next to the opening at the time of its aperture. This effect is also present for triangles. However, triangles form the arches very close to the orifice. As a consequence, the change in clogging probability is not as dramatic for triangles as it is for squares. Also pentagons and hexagons

J. Stat. Mech. (2018) 113201

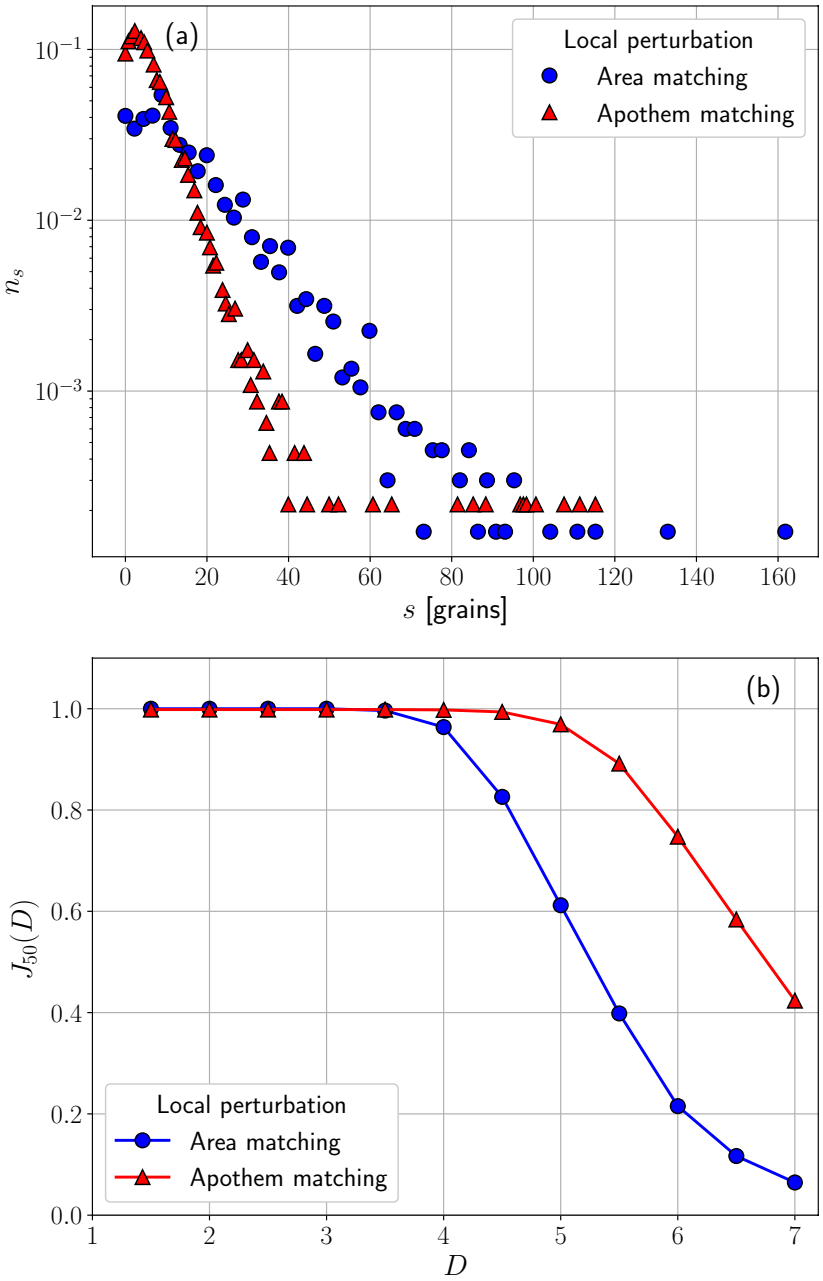

Figure 9. Clogging for triangular particles of different sizes. (a) Avalanche size distribution for triangles with same area as the disks (blue circles) and triangles with same apothem as the disks (red triangles) for an aperture $D = 4.0$. (b) Clogging probability as a function of D for the same triangular particles for $N = 50$.

are affected significantly (see arch vertical position in figure 8). As a result, squares, pentagons and hexagons increase their clogging probability to a large extent when the global protocol is used, leaving triangles in the third place of the shapes most likely to clog for this protocol.

J. Stat. Mech. (2018) 113201

5. Effect of the size-matching criterion

Although we have compared grains of different shapes keeping the mass (area) constant, other criteria may be used. For example, the diameter or the perimeter could be used as the conserved parameter for all particle shapes. As we have shown for the flow rate through large apertures in a previous study (see [19]), this choice can alter the results to a large extent, in particular for triangular grains.

As an example, we plot in figure 9 the avalanche size distribution and the clogging probability for two possible sizes of triangles. In one case the triangles have the same area as the reference disks and in the other the triangles present the same apothem as the disks radius. As we can see, the avalanche sizes are smaller for the apothem-matching triangles since these particles are considerably larger than the area-matching triangles. Accordingly, the clogging probability for the apothem-matching triangles is significantly higher (see figure 9(b)).

What size-matching criterion should be used to compare particles of different shapes depends on the particular application in mind [19]. If particles can be manufactured in any shape but the total mass of each grain needs to be conserved due to design or cost constraints, the mass-matching criterion must be used. If the mass of the grains can be changed but particles are required to have a given apothem, then the apothem-matching becomes mandatory as a criterion.

6. Conclusions

We have shown that grains having polygonal shapes present significant differences in their clogging probability when they flow through small apertures. In general, the lower the number of vertexes, the larger is their tendency to clog. However, triangles and squares display peculiar behaviors depending on the protocol used to trigger avalanches. Avalanches obtained by filling the container and then opening the orifice tend to favor preferentially the clogging of squares. Avalanches triggered by removing some grains from the arch of a previous clog tend to favor the clogging of triangles. This is due to the fact that squares tend to form arches at high vertical positions, while triangles build up arches close to the orifice. Arches broken at a high placement lead to large discharges since the grains fall through the opening with high kinetic energy thanks to the long empty channel left beneath the arch.

For the shapes studied, we have observed that the avalanche size distributions present exponential tails as it has been observed for circular and spherical grains in the past. However, the mean avalanche size for polygons (other than heptagons) grows much slower with aperture width if compared with disks. The results for heptagons suggest that polygons with larger number of vertexes may have a response comparable with disks in terms of clogging. It is worth pointing out that in other phenomena (such as compaction under tapping [20]) adding vertexes does not necessarily reduce the response of the system to the one observed for disks.

We have observed that there is some spread in the results for mean avalanche sizes for disks in the literature. Although the focus of this work is on the response of

J. Stat. Mech. (2018) 113201

polygonal grains, we suggest that an effort should be made in the community to reconciliate results for disks, to make experiments and simulations reproducible and so set a benchmark for future studies on clogging.

We have shown that the criterion used to compare particles of different shapes is an important point to consider. As an example, if triangular grains must have the same mass as disks, the resulting triangle would be smaller and less prone to clogging than if the apothem must coincide with the disks radius. This should be considered in view of the particular applications.

Finally, we have seen that the ability of the particles to form side-to-side contacts is not correlated with their clogging probability. However, these special contacts may impact on the stability of the clogging arches.

Acknowledgments

We thank A Garcimartín, and I Zuriguel for valuable discussions. This work has been supported by ANPCyT (Argentina) through grant PICT 2012-2155 and UTN (Argentina) through grants PID MAUTNLP-2184 and PID IFI-1871.

References

[1] Zuriguel I, Garcimartín A, Maza D, Pugnaloni L A and Pastor J M 2005 *Phys. Rev.* E **71** 051303
[2] Janda A, Zuriguel I, Garcimartín A, Pugnaloni L A and Maza D 2008 *Eur. Phys. Lett.* **84** 44002
[3] Thomas C C and Durian D J 2015 *Phys. Rev. Lett.* **114** 178001
[4] Magalhães C F M, Moreira J G and Atman A P F 2010 *Phys. Rev.* E **82** 051303
[5] Zuriguel I 2014 *Pap. Phys.* **6** 060014
[6] Mankoc C, Garcimartín A, Zuriguel I, Maza D and Pugnaloni L A 2009 *Phys. Rev.* E **80** 011309
[7] Janda A, Maza D, Garcimartín A, Kolb E, Lanuza J and Clément E 2009 *Europhys. Lett.* **87** 24002
[8] Zuriguel I *et al* 2014 *Sci. Rep.* **4** 7324
[9] Pastor J M, Garcimartín A, Gago P A, Peralta J P, Gómez C M, Ferrer L M, Maza D, Parisi D R, Pugnaloni L A and Zuriguel I 2015 *Phys. Rev.* E **92** 062817
[10] Patterson G A, Fierens P I, Sangiuliano Jimka F, Konig P G, Garcimartín A, Zuriguel I, Pugnaloni L A and Parisi D R 2017 *Phys. Rev. Lett.* **119** 248301
[11] To K, Lai P-Y and Pak H K 2001 *Phys. Rev. Lett.* **86** 71
[12] Garcimartín A, Zuriguel I, Pugnaloni L A and Janda A 2010 *Phys. Rev.* E **82** 031306
[13] Ashour A, Trittel T, Borzsonyi T and Stannarius R 2017 *Phys. Rev. Fluids* **2** 123302
[14] Lumay G, Schockmel J, Henández-Enríquez D, Dorbolo S, Vandewalle N and Pacheco-Vázquez F 2015 *Pap. Phys.* **7** 070013
[15] Hong X, Kohne M, Morrell M, Wang H and Weeks E R 2017 *Phys. Rev.* E **96** 062605
[16] Ashour A, Wegner S, Trittel T, Borzsonyi T and Stannarius R 2017 *Soft Matter* **13** 402
[17] Box2D Physics Engine www.box2d.org
[18] Catto E 2010 *Iterative dynamics with temporal coherence* http://box2d.org/files/GDC2005/IterativeDynamics.pdf (Accessed: October 2018)
[19] Goldberg E, Carlevaro C M and Pugnaloni L A 2015 *Pap. Phys.* **7** 070016
[20] Carlevaro C M and Pugnaloni L A 2011 *J. Stat. Mech.* P01007
[21] Goldberg E, Carlevaro C M and Pugnaloni L A 2017 *EPJ Web Conf.* **140** 06009
[22] Zuriguel I, Pugnaloni L A, Garcimartín A and Maza D 2003 *Phys. Rev.* E **68** 030301
[23] Uñac R O, Vidales A M and Pugnaloni L A 2012 *J. Stat. Mech.* P04008
[24] Pugnaloni L A, Barker G C and Mehta A 2001 *Adv. Complex Sys.* **4** 289
[25] Pugnaloni L A and Barker G C 2004 *Physica* A **337** 428
[26] Arevalo R, Maza D and Pugnaloni L A 2006 *Phys. Rev.* E **74** 021303
[27] To K 2005 *Phys. Rev.* E **71** 060301
[28] Gella D, Maza D, Zuriguel I, Ashour A, Arévalo R and Stannarius R 2017 *Phys. Rev. Fluids* **2** 084304
[29] Pérez G 2008 *Pramana* **70** 989

[30] Arévalo R and Zuriguel I 2016 *Soft Matter* **12** 123
[31] Roth L K and Jaeger H M 2016 *Soft Matter* **12** 1107
[32] Guerrero B V, Pugnaloni L A, Lozano C, Zuriguel I and Garcimartín A 2018 *Phys. Rev.* E **97** 042904
[33] Merrigan C, Birwa S K, Tewari S and Chakraborty B 2018 *Phys. Rev.* E **97** 040901
[34] López-Rodríguez D, Zuriguel I and Maza D 2017 *EPJ Web Conf.* **140** 03033

J. Stat. Mech. (2018) 113201